Aerothermal Analysis and Environment Predictions for the Mars Sample Retrieval Lander (SRL)

Suman Muppidi[a], Dinesh Prabhu[b], David Saunders[b], Ryan McDaniel[a], Rathakrishnan Bhaskaran[b], David Kinney[a], Kaelan Hansson[b], Alireza Mazaheri[c] , Karl Edquist[c]

[a]*NASA Ames Research Center, Moffett Field, California 95045, USA*
[b]*AMA, Inc. at NASA Ames Research Center, Moffett Field, CA 94035, USA*
[c]*NASA Langley Research Center, Hampton, Virginia, 24681, USA*

Mars Sample Retrieval Lander (SRL) is the next mission to Mars, and an integral part of the proposed Mars Sample Return (MSR) Program. Aerothermal Analysis of the SRL capsule takes advantage of the design and analysis of the Mars Science Laboratory and the Mars 2020 missions, findings from the MEDLI and MEDLI2 heatshield instrumentation campaigns, and developments in predictive capabilities over the last 20 years. In particular, SRL is being designed to enter the Mars atmosphere at velocities as high as 8 km/s, which would be the highest for a Mars entry, and is expected to encounter additional shock layer radiation physics compared to previous missions to Mars. This paper presents the status of analysis including the overall methodology, models and assumptions of the aerothermal environment predictions, with a focus on differences from the approaches and modeling used for Mars 2020 and MSL.

I. Introduction

NASA and ESA are jointly planning a Mars Sample Return (MSR) campaign, consisting of multiple mission elements, to bring bring back samples currently being collected on Mars by the NASA Perseverance rover[1]. A key element of the MSR architecture is the Sample Retrieval Lander (SRL), which would land a Mars Launch System (MLS) designed to carry the collected samples into Mars orbit, and delivered to Earth by subsequent mission elements. This mission architecture has been studied for several years, and provides a means to meet one of the highest objectives in the past several Planetary Science Decadal Surveys[2]. SRL is being designed to land the heaviest payload yet (nearly 1100 kg capability for Mars2020 vs 2900 kg for SRL), on the surface of Mars, and has a significantly higher ballistic coefficient.

Figure 1 shows an overview of the SRL EDL Concept of Operations (ConOPS), starting from the Entry Interface when the spacecraft first encounters the Martian atmosphere, through touchdown of the lander. Aspects of the ConOPS are similar to those of MSL and Mars2020: the cruise stage separates 10 minutes prior to Entry Interface, and is followed by the ejection of cruise balance mass to achieve the design angle of attack. The spacecraft experiences the heat pulse at a constant Lift/Drag ratio. At the end of the heat pulse, the spacecraft returns to a near-zero degree angle of attack by ejecting entry balance masses. Next, the parachute lid is ejected, and is followed closely by parachute deployment. Computational Fluid Dynamics (CFD) analysis is used through the spacecraft design process in multiple ways:

(a) prediction of the surface aerothermal environment, and design of the Thermal Protection System (TPS)
(b) prediction of surface pressure fields to help design separation and ejection mechanisms
(c) inputs required for planetary protection
(d) inputs to enable detailed backshell design choices (e.g. RCS thrusters, fasteners, gaps, seals)

The focus of this paper is the Entry segment of the ConOPS.

Aerothermal analysis of SRL relies strongly on analyses and testing performed for the Mars Science Laboratory[3] (MSL) and Mars2020[4,5] missions, and the lessons learned via Entry Instrumentation efforts MEDLI[6] and MEDLI2[7]. MSL was the largest and heaviest Mars spacecraft to date, flying a lifting entry; its design and aerothermal analysis was supported by a wind tunnel test campaign as a means to gather data and validate

computational tools and models. MEDLI and MEDLI2 included instrumentation through pressure and in-depth temperature measurements across the heatshield, and direct heating measurements on the backshell (MEDLI2). MEDLI and MEDLI2 yielded valuable data that have been, and continue to be, key to gaining confidence in predictive capabilities, and make modifications where necessary.

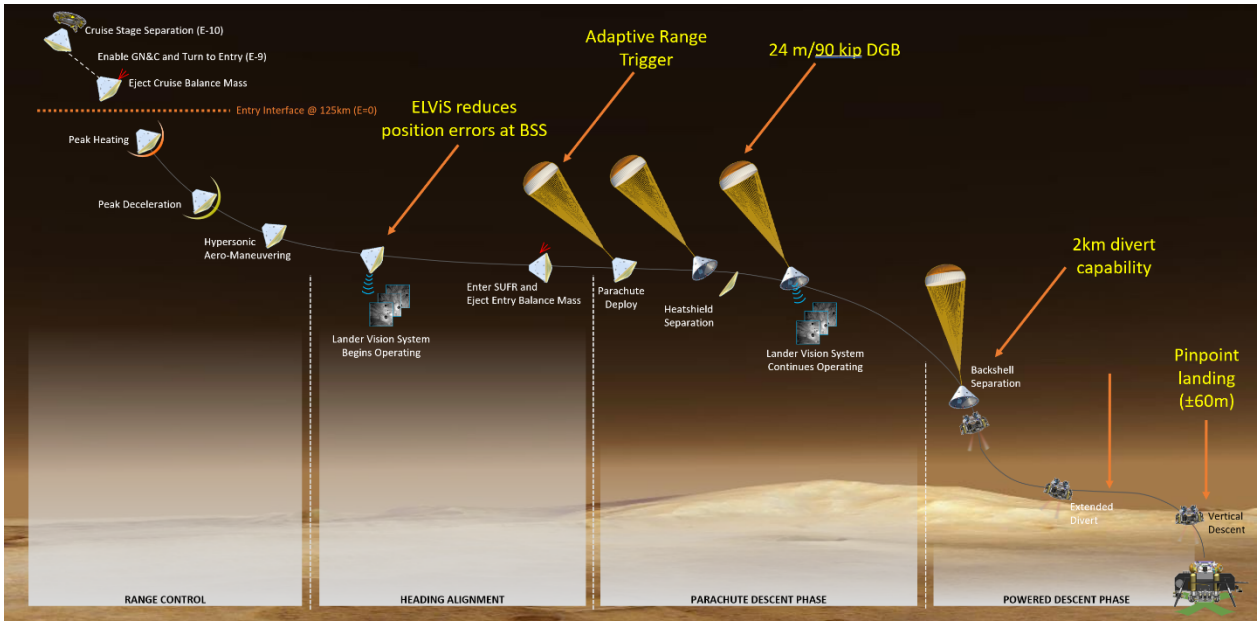

Fig. 1 SRL EDL Concept of Operations

The SRL mission is in the Preliminary Design stage. Aspects of the design are still changing, including geometry and trajectory space. Figure 2 shows two of the SRL geometry options used for the analysis in this paper, compared with MSL/Mars 2020. The figure also shows the notional TPS split lines. Similar to MSL and M2020, the SRL capsule is covered by PICA, SLA-561V and Acusil-II over the heatshield, backshell and the parachute cone assembly respectively.

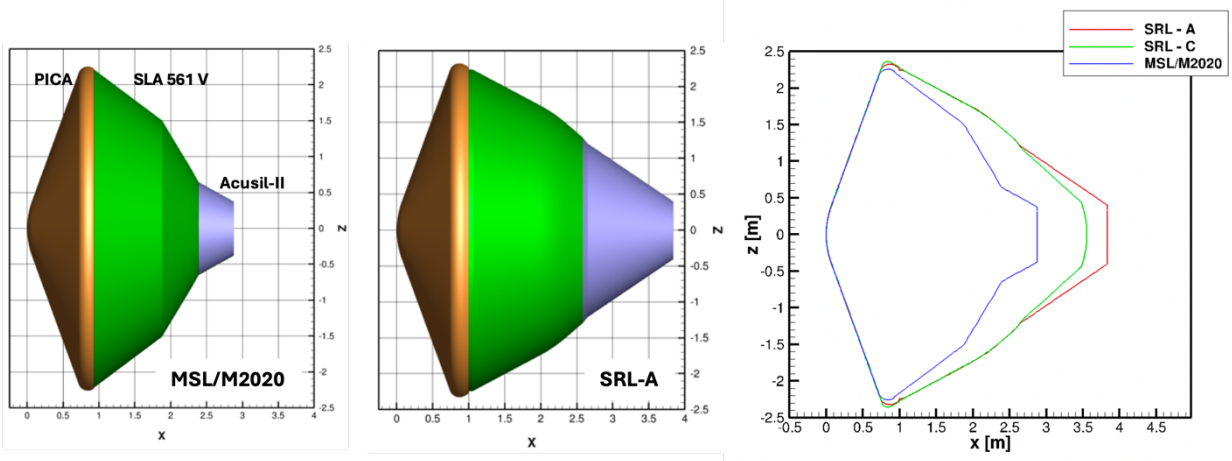

Fig. 2 Geometry Comparison. All dimensions in meters, and shown in the aerothermal reference frame. X-Z is the plane of symmetry; +Z is windward side; -Z is the leeward side.

SRL is currently being designed to accommodate two launch opportunities: 2028 and 2031. For the purposes of this paper, the largest difference in the two opportunities is the entry velocity. Figure 3 shows representative SRL trajectories for both opportunities (and entry velocities 5.4 km/s and 7.8 km/s), co-plotted with as-flown (Best

Estimated) trajectories of MSL and M2020. Due to the higher ballistic coefficient, both SRL trajectories experience a higher dynamic pressures, which translates to higher surface pressures. Compared to MSL and Mars2020, the heatshield TPS is expected to experience twice the stagnation pressure, which impacts the TPS verification and test program. Also, the density-velocity plot shows that for a given velocity, SRL flies through a denser atmosphere, which translates to higher heating. To achieve the EDL timeline necessary, SRL flies at a higher angle of attack at hypersonic conditions, of nearly -20° as compared to about -16° of MSL/M2020.

Table. 1 SRL Design trajectory parameters compared to MSL and Mars2020, as-flown trajectories.

	MSL BET	Mars 2020 BET	SRL (2028)	SRL (2031)
Entry Mass (kg)	3153	3369	5700	5900
Entry Speed (m/s)	5845	5334	5400	7700
Entry Flight Path Angle (deg)	-15.12	-15.5	-15.0	-12.5
Peak Dynamic Pressure (Pa)	15,915	14,685	~ 26000	~28000
Ballistic Coefficient (kg/m2.s)	~140	~150	~245	~245

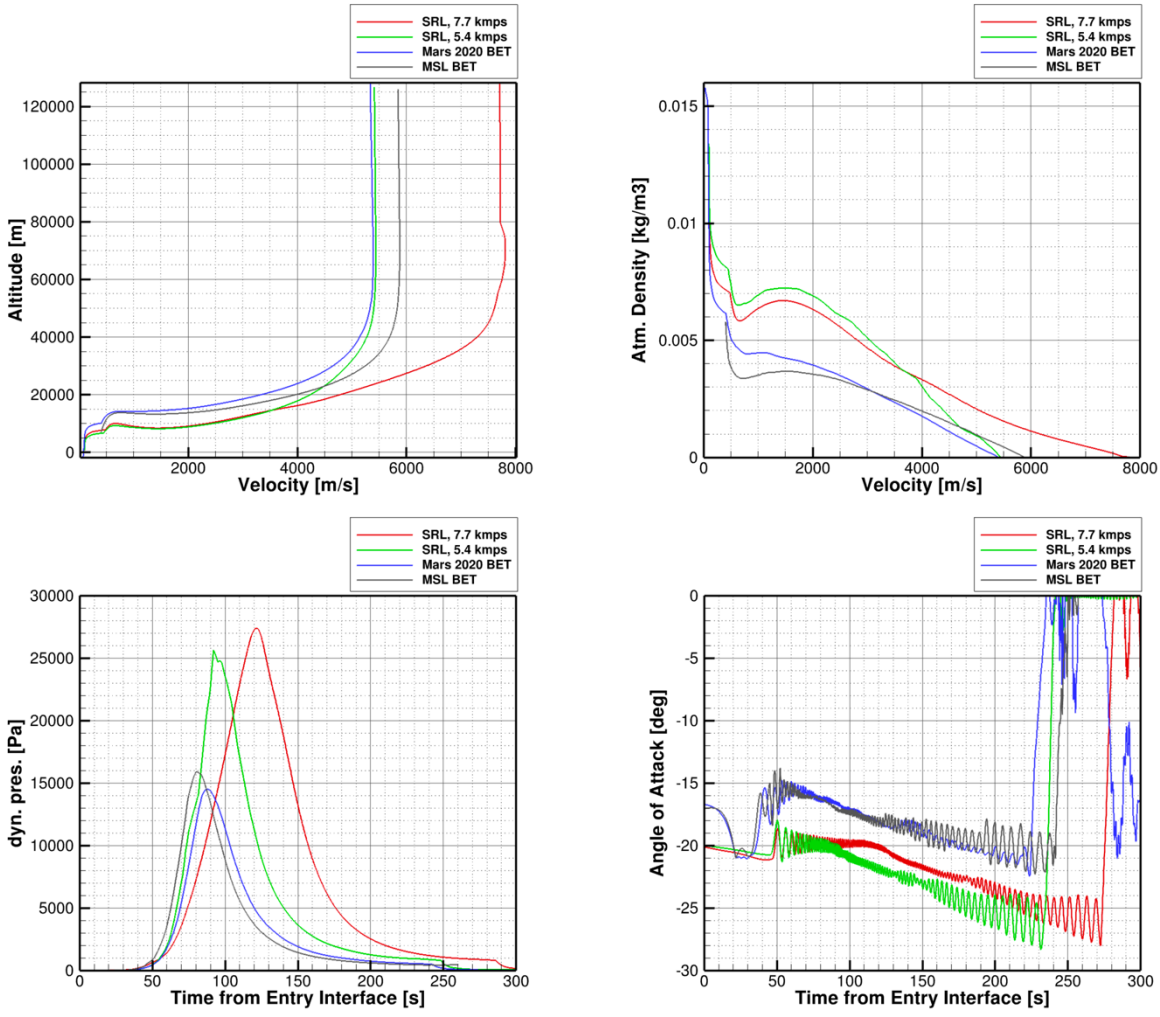

Fig. 3 Image shows two SRL trajectories (with entry velocities 5.4 km/s and 7.8 km/s), compared to as-flown MSL and Mars2020 trajectories. The impact of the higher ballistic coefficient is apparent.

The purpose of this paper is to present the aerothermal analysis methodology used for SRL, identify differences from MSL/M2020 (if any), and provide the justification (where appropriate). The paper is organized as follows. Section II provides a brief overview of the various inputs and steps involved in the prediction of the aerothermal environments (primarily convective and radiative heating rate, along with parameters such as pressure, shear stress, and film coefficient necessary for TPS design, sizing analyses, and test planning). Section III lays out the different models used as part of aerothermal analyses. Section IV presents results, showing current prediction of aerothermal environments for the design of SRL.

II. Scope and Framework

This section briefly presents the scope of the aerothermal environment analysis, and the general framework. The primary objective of aerothermal analysis presented here is to generate and provide time traces of aerothermal environments (convective and radiative heat transfer rates) needed for TPS material response analysis and thickness determination. Reference [8] provides a comprehensive overview of the TPS sizing and design process for Mars 2020. As mentioned there, the analysis process is designed to account for aerothermal uncertainties, and trajectory dispersions.

Figure 4 illustrates the aerothermal analysis workflow. For a given geometry and trajectory, real gas flow solvers (DPLR/LAURA) are used to calculate shock-aligned volumetric flowfields and surface convective heating environments for a set of discrete trajectory points (freestream conditions). CFD flowfields are post-processed to estimate a surface roughness augmentation (where appropriate), and to provide inputs to the shock layer radiation solvers (NEQAIR/HARA). Heating (convective, radiative) distributions, along with the aeroshell substructure, are used to identify body points of interest, that could potentially drive TPS design. Aerothermal indicators, curve fits based on trajectory parameters, are derived for each of these body points, and used to generate time-traces of the environment (e.g. radiative heating, convective heating, film coefficient, surface pressure, shear stress, edge enthalpy) along the trajectory (or a set of trajectories) of interest. As mentioned above, SRL is being designed to accommodate both a 5.4 km/s and a 7.8 km/s entry velocity trajectory. This paper will make use of analysis and results along both these trajectories to highlight elements of the workflow. Table 2 provides the discrete freestream conditions used for the analysis presented in this paper.

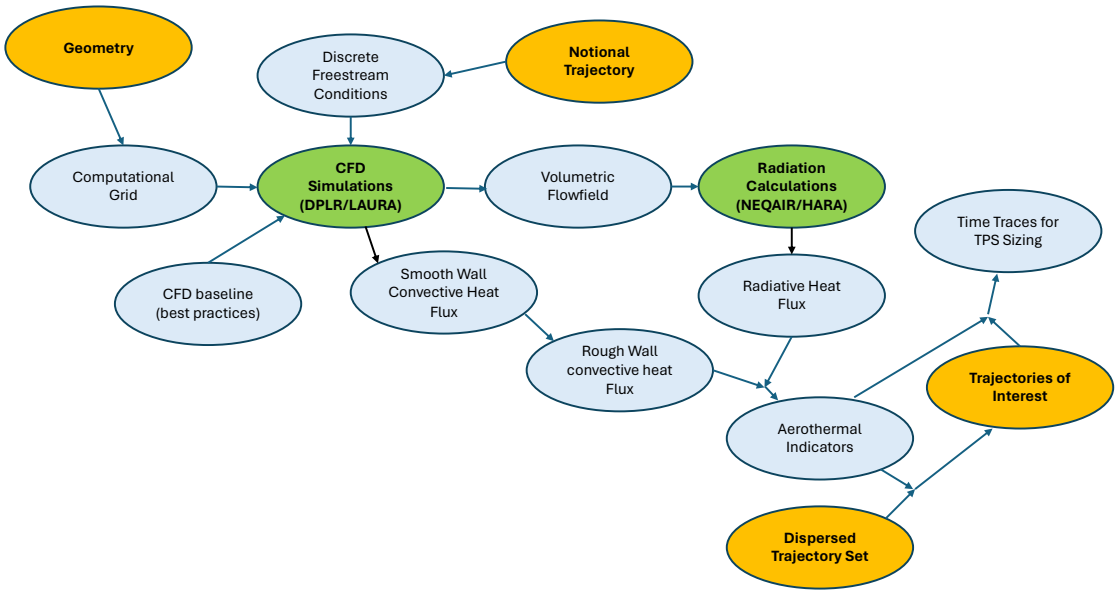

Fig. 4 Schematic work flow of the aerothermal analysis process..

Table 2 Freestream conditions along the two nominal trajectories used for the analysis presented in this paper, correspond to the two SRL trajectories shown in Figure 3. Entry Interface is at time 540s for both.

Entry Velocity **5.4 km/s**					Entry Velocity **7.8 km/s**				
Entry Flight Path Angle **-15.0 deg**					Entry Flight Path Angle **-12.0 deg**				
Entry Mass **5700 kg**					Entry Mass **5900 kg**				
Time [s]	**Density [kg/m3]**	**Velocity [m/s]**	**Temperature [K]**	**Angle of Attack [deg]**	**Time [s]**	**Density [kg/m3]**	**Velocity [m/s]**	**Temperature [K]**	**Angle of Attack [deg]**
580	6.2376E-06	5436.52	151.4	-20	580	5.9750E-06	7802.28	134.72	-20
589	2.5583E-05	5435.12	151.7	-20	585	1.1760E-05	7811.25	143.16	-20
596	7.4925E-05	5419.51	152.39	-20	594.5	2.9074E-05	7753.76	147.40	-20
604	2.3481E-04	5359.64	152.38	-20	600	4.6781E-05	7681.62	147.03	-20
612	6.2115E-04	5176.78	152.1	-20	607	9.2439E-05	7612.00	138.53	-20
619	1.0799E-03	4869.93	159.19	-20	614	1.7122E-04	7513.40	137.62	-20
625	1.7057E-03	4521.74	167.42	-20	620	2.6073E-04	7374.86	144.48	-20
628	2.2536E-03	4294.5	173.01	-20	630.1	4.8088E-04	7000.30	158.30	-20
632	3.2710E-03	3933.57	182.77	-20	636	6.6608E-04	6682.83	166.02	-20
641	5.0095E-03	3055.4	192.6	-20	639.2	7.9147E-04	6480.34	170.09	-20
648	6.1226E-03	2472.23	197.29	-20	655	1.9192E-03	5132.71	185.42	-20
656	6.9400E-03	1975.68	199.91	-20	662	2.8573E-03	4379.62	191.85	-20
665	7.2257E-03	1587.96	201.18	-20	680	5.2191E-03	2700.18	201.84	-20
680	7.1681E-03	1193.81	200.75	-20	700	6.6382E-03	1653.71	205.98	-20

III. Aerothermal Analysis for SRL

Prediction of the flowfield around the capsule, and the surface environments for SRL are chiefly carried out through the codes DPLR[9] and NEQAIR[10], owned and maintained by NASA Ames Research Center. Independent Verification and Validation, is performed using LAURA[11] and HARA[12], maintained by NASA Langley Research Center. CFD simulations and solution quality checks are performed using best practices learned through past missions, including MSL and Mars2020, such as (a) tailoring of the computational mesh to the bow shock, (b) inclusion of sufficient (5-7 vehicle diameters) downstream distance for reliable aft body radiation predictions, and (c) appropriate clustering of the computational mesh near the shock and the surface. Figure 5 shows representative computational meshes used for the CFD analyses.

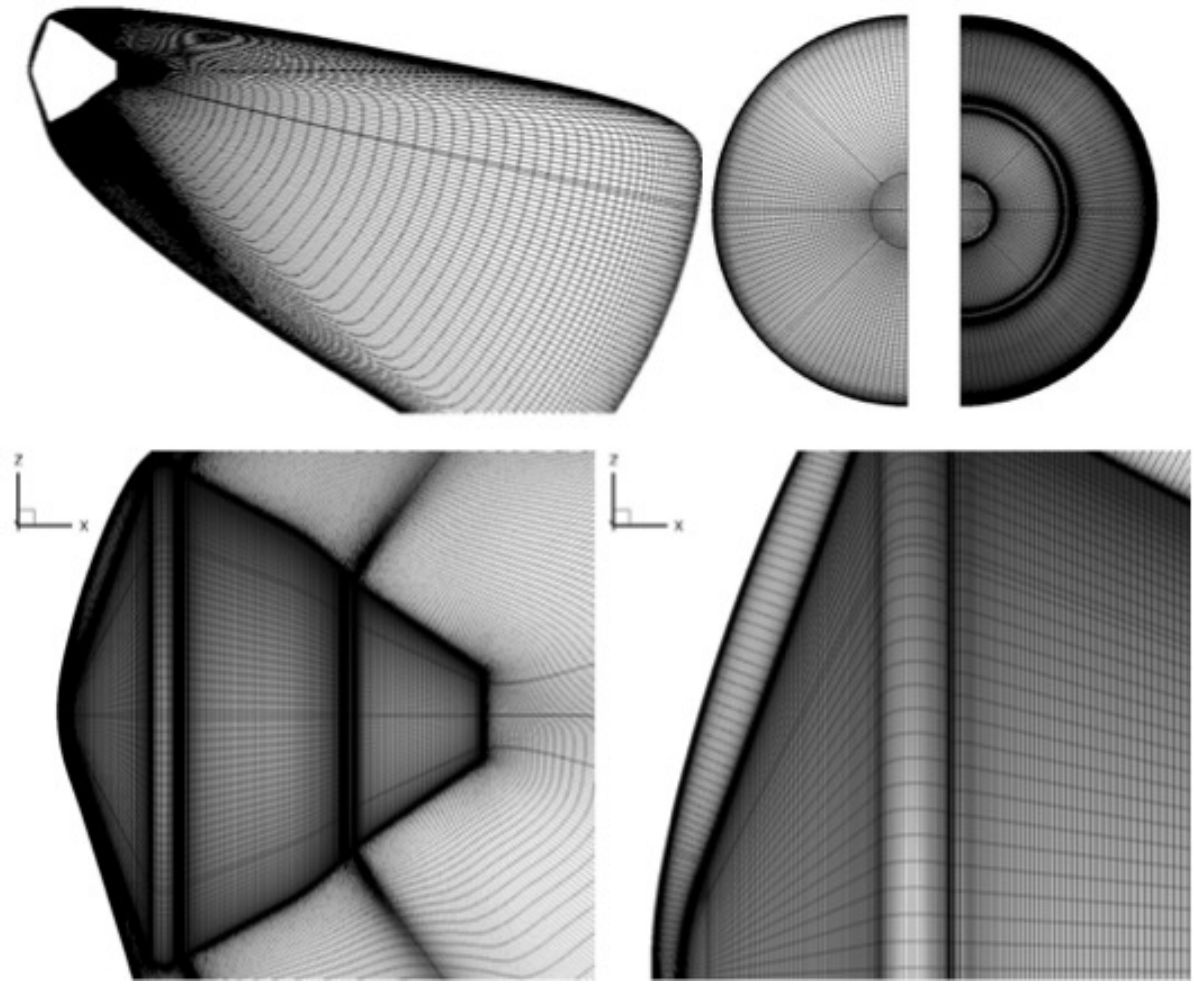

Fig. 5 Representative images of the computational mesh used for the CFD. Note the downstream length of the domain for adequate aft-body radiation estimates, and the clustering of the mesh near the shock, the boundary layer, and in regions of high surface curvature.

A. Chemistry

The atmosphere of Mars is composed of CO_2 and N_2, with trace amounts of Argon. The Navier-Stokes solvers DPLR and LAURA account for thermal and chemical non-equilibrium, and solve finite rate chemistry, utilizing a library of available chemistry models. Analysis for MSL and Mars2020 were based on an 8-species Mars Chemistry model[13,14]. Johnston and Brandis[15] proposed an updated chemistry mechanism that yields improved comparisons against non-equilibrium radiation experiments in the Electric Arc Shock Tube, NASA Ames Research Center. This chemistry model can be implemented as a 10-species, 20-reaction variant in the absence of ionization, or an 18-species 34-reaction model that includes ionization reactions. When SRL design was focused only on the 2028 opportunity with an entry velocity less than 6 km/s, the aerothermal analysis employed the non-ionizing, 10 species model. Since the incorporation of higher entry velocities into the design space, and the expectation of significant ionization at these entry velocities, the analysis now employs the more appropriate 18-species mechanism.

Table 3. List of species that make up the chemistry models.

Mechanism	Species
8-species[13]	CO_2,CO,N_2,O_2,NO,C,N,O
10-species[15]	CO_2, CO, N_2, O_2, NO, C_2, CN, C, N, O
18-species[15]	CO2, CO, CO^+, C2, N2, O2, $O2^+$, NO, NO^+, CN, C, C^+, N, N^+, O, O^+, Ar, e

Table 3 indicates the species that make up the three chemistry models mentioned above, with each row highlighting the species that are new compared to the row above. Figure 6 shows profiles of temperatures (translational, and vibrational) and some selected species concentrations (as number density) along the stagnation line, from one of the simulations [freestream velocity 6.48 km/s and density 7.9147e-4 kg/m3 along the 7.8 km/s entry velocity trajectory]. These profiles indicate that at this condition, most of the stagnation line is in thermal equilibrium except at the shock, where the two temperatures are different. Also, the neutral species appear to have reached a chemical equilibrium post shock (as evidenced by almost-constant concentration between the shock and the boundary layer), whereas the charged species continue to react along the stagnation line.

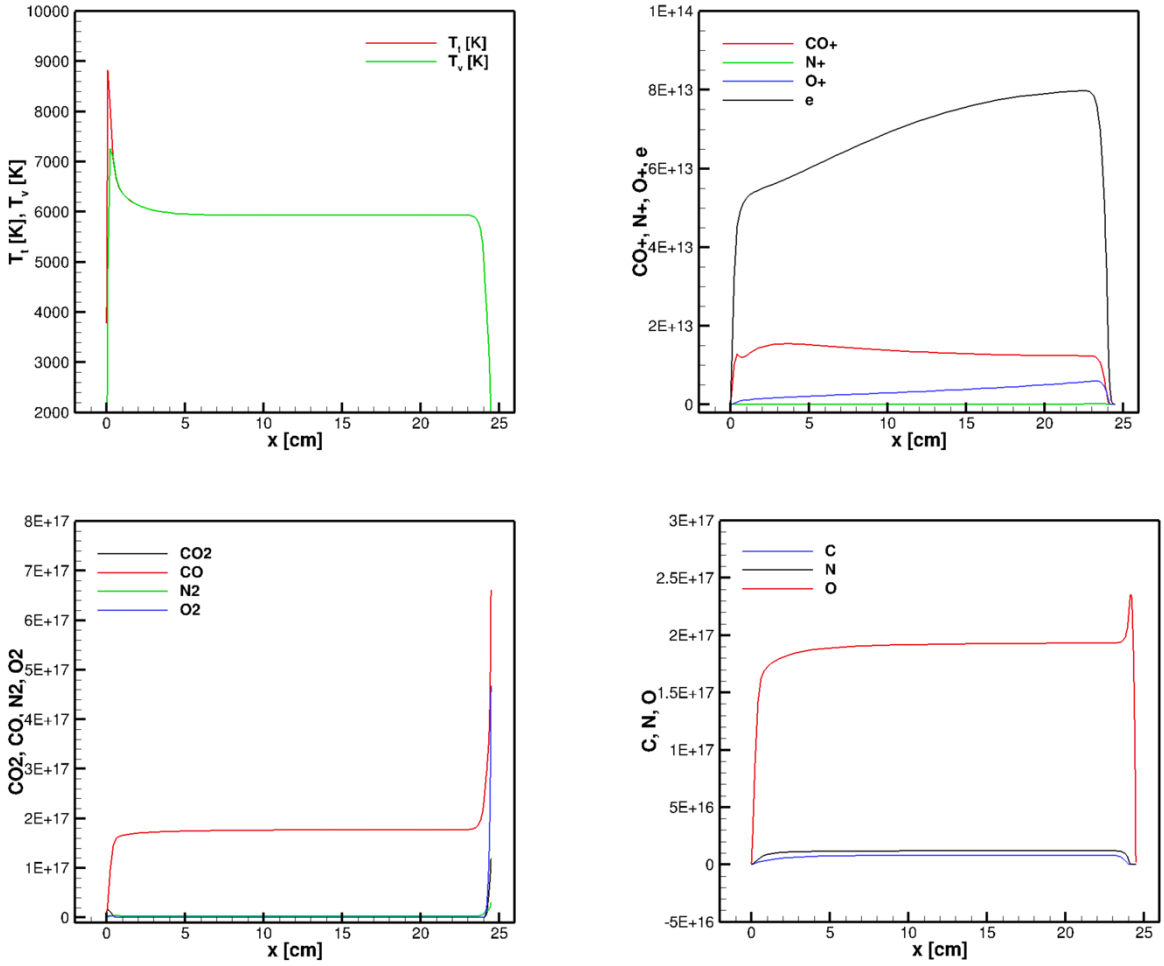

Fig. 6 Stagnation line profiles from a example simulation using the 18 species chemistry, showing the regions of ionization, nonequilibrium, shock and boundary layer.
Freestream velocity 6.48 km/s and density 7.9147e-4 kg/m3

B. Turbulence Modeling

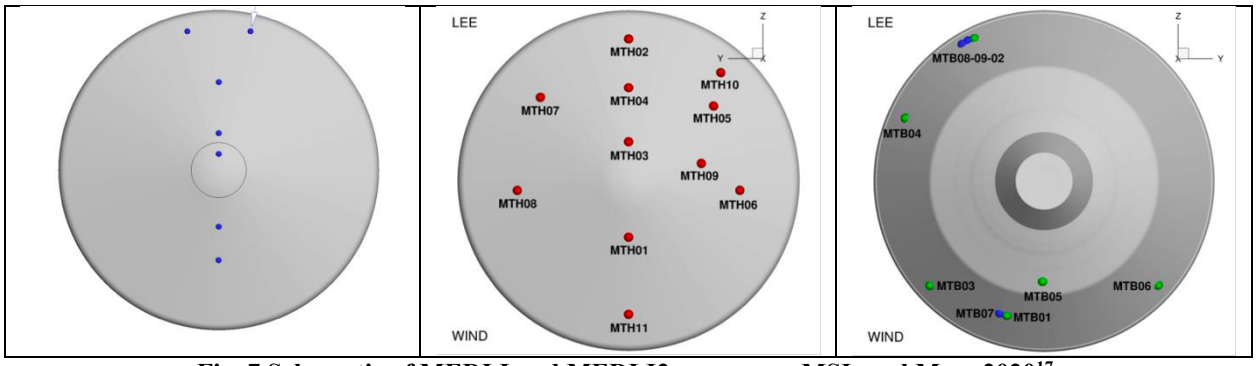

Fig. 7 Schematic of MEDLI and MEDLI2 sensors on MSL and Mars 2020[17].

According to Reference [3], MSL was the first spacecraft to Mars that was expected to experience turbulent flow on the heatshield/forebody prior to peak heating. Prior missions likely observed laminar-to-turbulent transition after peak heating, if at all. As a result, MSL and Mars2020 were designed to fully turbulent environments on the heatshield. CFD simulations employed the Baldwin-Lomax[16] turbulence model following a detailed wind tunnel test campaign[3]. MEDLI and MEDLI2 (Figure 7) returned data indicating that the heatshield indeed transitioned to turbulent flow, and that transition began prior to time of peak heating. Signs of transition appear first on the lee side plugs (as would be expected), almost immediately followed by plugs on the mid-flank and near-nose. Reference [17] used the times of transition from MEDLI2 to evaluate various transition corelations, and conclude that heatshield transition was likely roughness induced and that none of the smooth-wall transitionl corelations capture the rapid progression of the turbulent transition front evidenced by flight data.

SRL is also expected to experience transition to turbulent flow on the heatshield during the entry pulse. Due to the heavier mass (and potentially higher velocity), transition is likely to occur earlier in the trajectory compared to MSL/Mars2020. As a result, SRL is being designed to a fully turbulent environment on the heatshield, but using a different turbulence model. Early SRL analysis indicated that the Baldwin-Lomax turbulence model results in anomalous high magnitudes of eddy viscosity in the inviscid flow region on the lee side. Investigations indicated this was due to a failure of the boundary layer edge search function for certain ranges of enthalpy difference (H_{wall}-H_{edge}), and is exacerbated by the choice of surface catalycity (see subsection D). The search for the boundary layer edge is an integral part of the Baldwin-Lomax turbulence model, and can be challenging at times (e.g. separated flows, and certain combinations of wall and edge enthalpies). SRL analysis employs SST[18] as the primary model for turbulent environment predictions, and Cebeci-Smith (reference) for Verification and Validation. Detailed CFD analysis of wind tunnel data was undertaken to understand the performance of the SST model, and to inform biases and uncertainties. The companion paper[19] contains more details.

MSL and Mars2020 were both designed using laminar flow analyses on the aft body, but with margin factors that account for the possibility of turbulent flow[20]. While MEDLI2 provided measurements on the backshell, the data were unable to determine if the flow transitioned[17]. In contrast, SRL is being designed to a fully turbulent flow on the aft body driven by its shape and angle of attack, both of which result in a longer attached flow region on the windward side. Note that commonly used criteria for transition to turbulence on a smooth surface ($Re_\theta, and\ Re_\theta/M_{edge}$) indicate a potential for turbulent flow. Also note that the aft body/backshell is not really smooth, as it contains features that could promote transition to turbulence.

Figure 8 shows symmetry line profiles of convective heat flux on the forebody/heatshield (left) and on the aft body (right). On the heatshield, peak laminar heating occurs on the windward shoulder, while the peak turbulent heating occurs near the lee side flank, consistent with the pre-flight expectations (and post-flight reconstruction) of both MSL and Mars 2020. On the aft body, most of the lee side is in a separated flow region, exhibiting lower convective heat fluxes relative to the wind side.

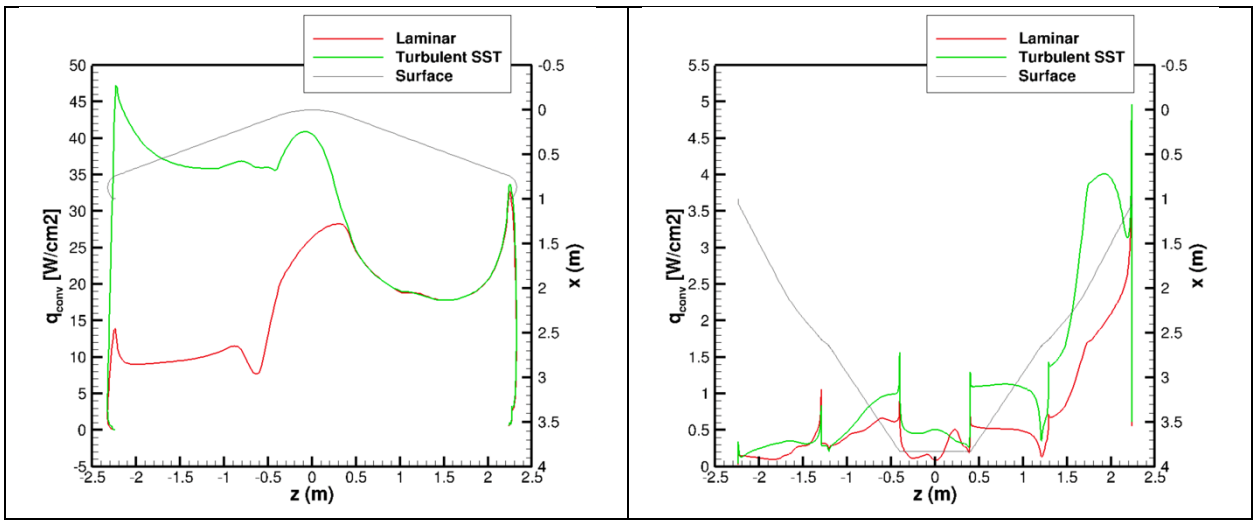

Fig. 8 Symmetry line profiles of (laminar and turbulent) convective heating on the forebody, and on the aftbody. Freestream velocity 4.87 km/s; density 1.0799e-3 kg/m3.

C. Effect of Angle of Attack

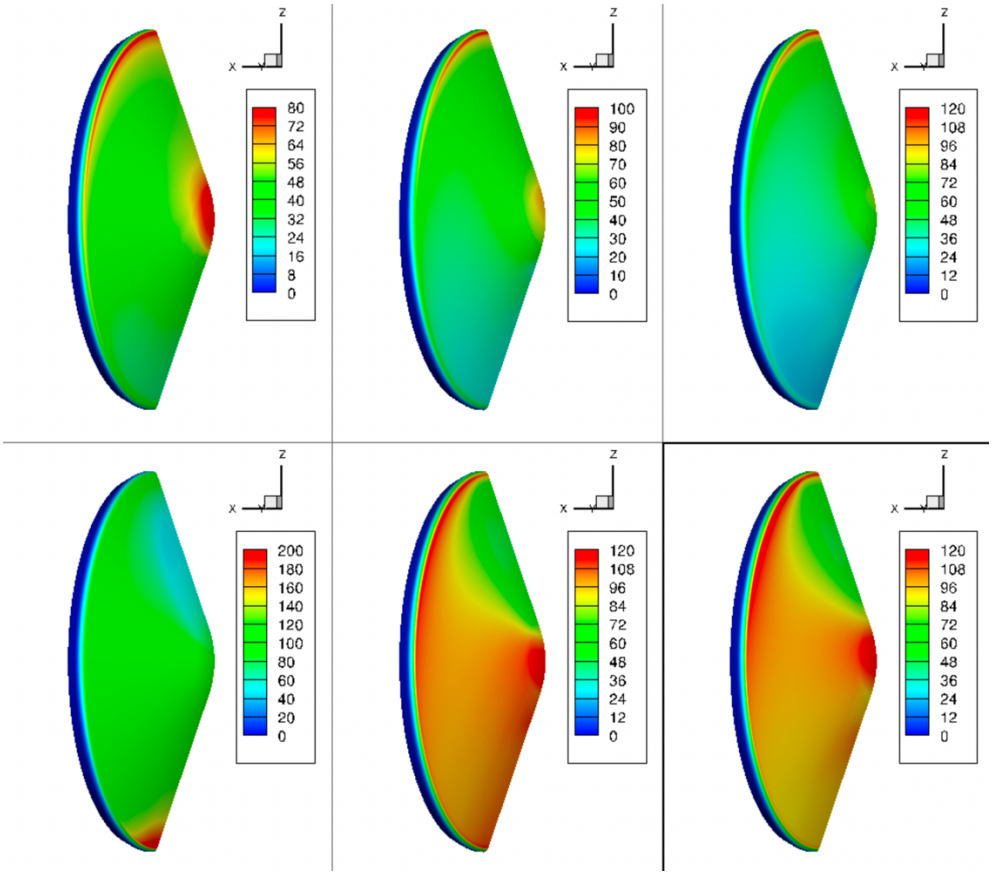

Fig. 9 Contours of (unmargined, smooth wall) convective heat flux at angles of attack: -15°, -20° and -25°. Top row is laminar flow, bottom row is turbulent flow. Freestream velocity 6.48km/s; density 7.9147e-4 kg/m3.

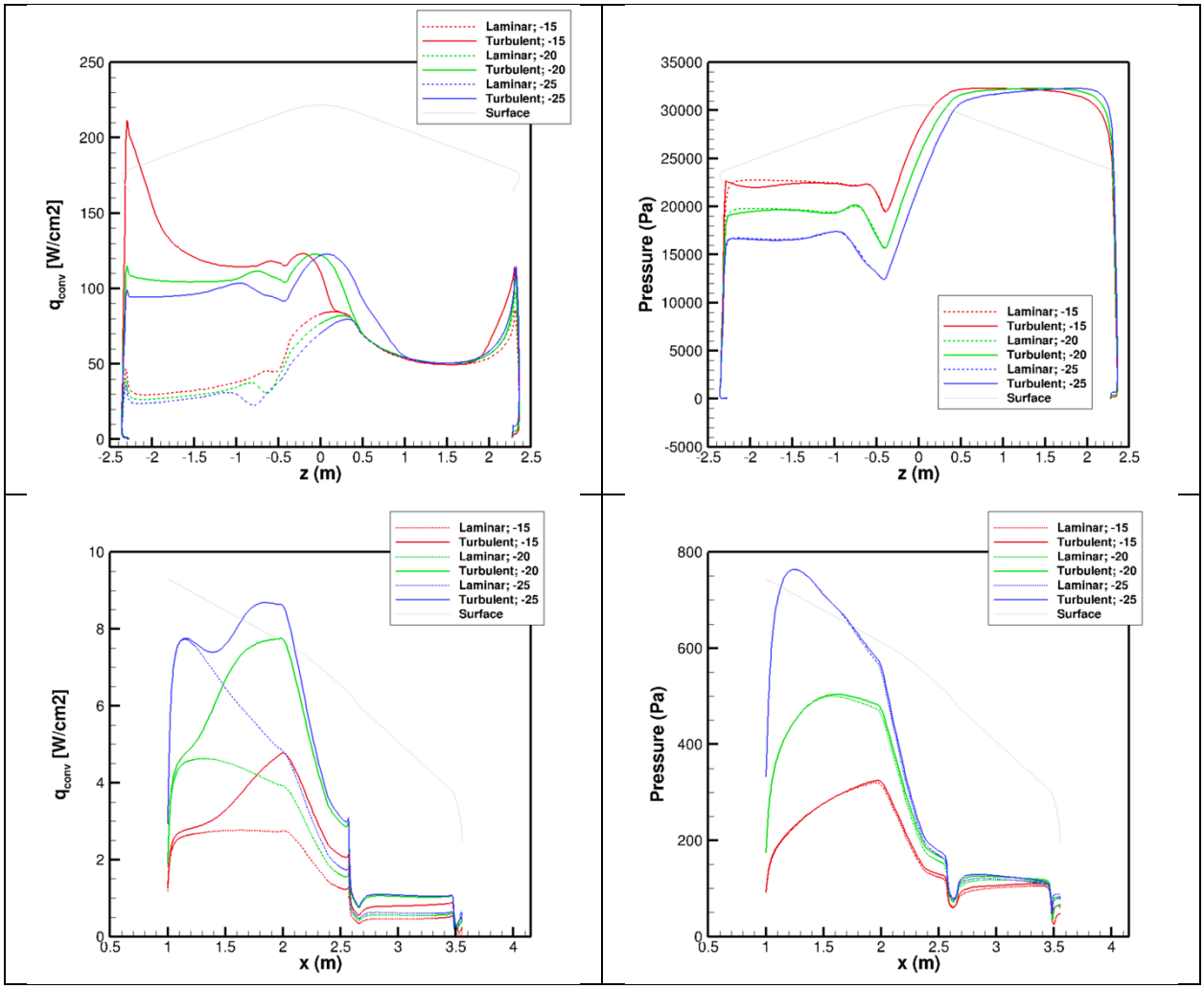

Fig. 10 Effect of angle of attack on the symmetry line profiles. Images show (smooth wall, unmargined) convective heating on the forebody (top row) and the windside aft body (bottom row). Freestream velocity 6.48km/s; density 7.9147e-4 kg/m3

Both MSL and Mars 2020 were designed to a Lift/Drag ratio (L/D) of 0.24[21], and a hypersonic angle of attack of nearly -16°. SRL is designed for an L/D of 0.3, which corresponds to an angle of attack of of nearly -20°. Preliminary simulations were focused on understanding the effect of angle of attack on the predicted aerothermal environment. Figures 9 and 10 contrast turbulent convective heating and surface pressure at three angles of attack: -15°, -20° and -25°. On the heatshield, -15° angle of attack results in the highest heating, and is consistent with the heating distributions from analysis of MSL and Mars 2020. At -20°, lee side peak heating drops significantly, and not much higher than the heating on the nose. At -25°, peak heating is observed near the nose. Surface pressure profiles show that (a) the stagnation point moves towards the windward shoulder with an increase in angle of attack, (b) the magnitude of stagnation pressure is the same for all three angles of attack, and (c) the lee side surface pressure is lower going from -15° to -20°, to -25°. Figure 10 also compares similar profiles, for the windward (attached) aft body environments. Here, increasing angle of attack results in higher surface pressures, and convective heating. The net effect of the change in angle of attack (from MSL/M2020's -16° to SRL's -20°) is decreased peak heating on the heatshield, and an increased peak heating on the back shell. Aerothermal analysis and subsequent TPS design account for these changes.

D. Surface Catalycity

Catalysis[22], by which the surface facilitates the recombination of species, can be a large contributor to convective heating. Catalytic state (and the appropriate catalytic treatment during analysis) is a function of the atmosphere, the

TPS surface, and the surface conditions such as temperature. Aerothermal analysis of MSL and Mars 2020 employed a "supercatalytic" assumption (for the PICA heatshield and the SLA-561 V backshell) in which the composition at the wall is forced to be that of the freestream, or the lowest enthalpy state, which is unphysical but conservative. Post-flight reconstruction and comparisons against MEDLI/MEDLI2[3] confirm the conservative nature of this assumption. SRL analysis models the heatshield and the backshell as *fully catalytic* to atom (and ion) recombination: homogenous catalysis ($O + O \longrightarrow O_2$; $N + N \longrightarrow N_2$). The parachute cone surface is covered by Acusil-II, and is treated as non-catalytic, similar to Mars 2020. Figure 11 compares the symmetry line profiles of convective heat flux and its components ($q_{conv} = q_T + q_D + q_R + q_V$). Note that the choice of catalysis model has a significant impact on the diffusive heatflux and the total convective heatflux (q_{conv} is predicted to be different by a factor of 2 at this freestream condition).

Figure also co-plots the film coeffient $[C_H = q_{conv}/(H_{wall} - H_{edge})]$ and shows that the impact of catalytic treatment on film coefficient is much smaller. As mentioned in [8], [23] and [24], TPS sizing analysis for the heatshield/forebody uses film coefficient and edge/recovery enthalpy, while that for the aftbody/backshell/parachute cone/lid uses heat flux(es) directly. The switch to catalytic treatment, therefore, significantly affects the backshell TPS sizing, but not the forebody/heatshield TPS sizing. Since most TPS testing requirements are based on predicted heat flux, however, the lower heat fluxes on the heatshield do affect the TPS testing and verification requirements.

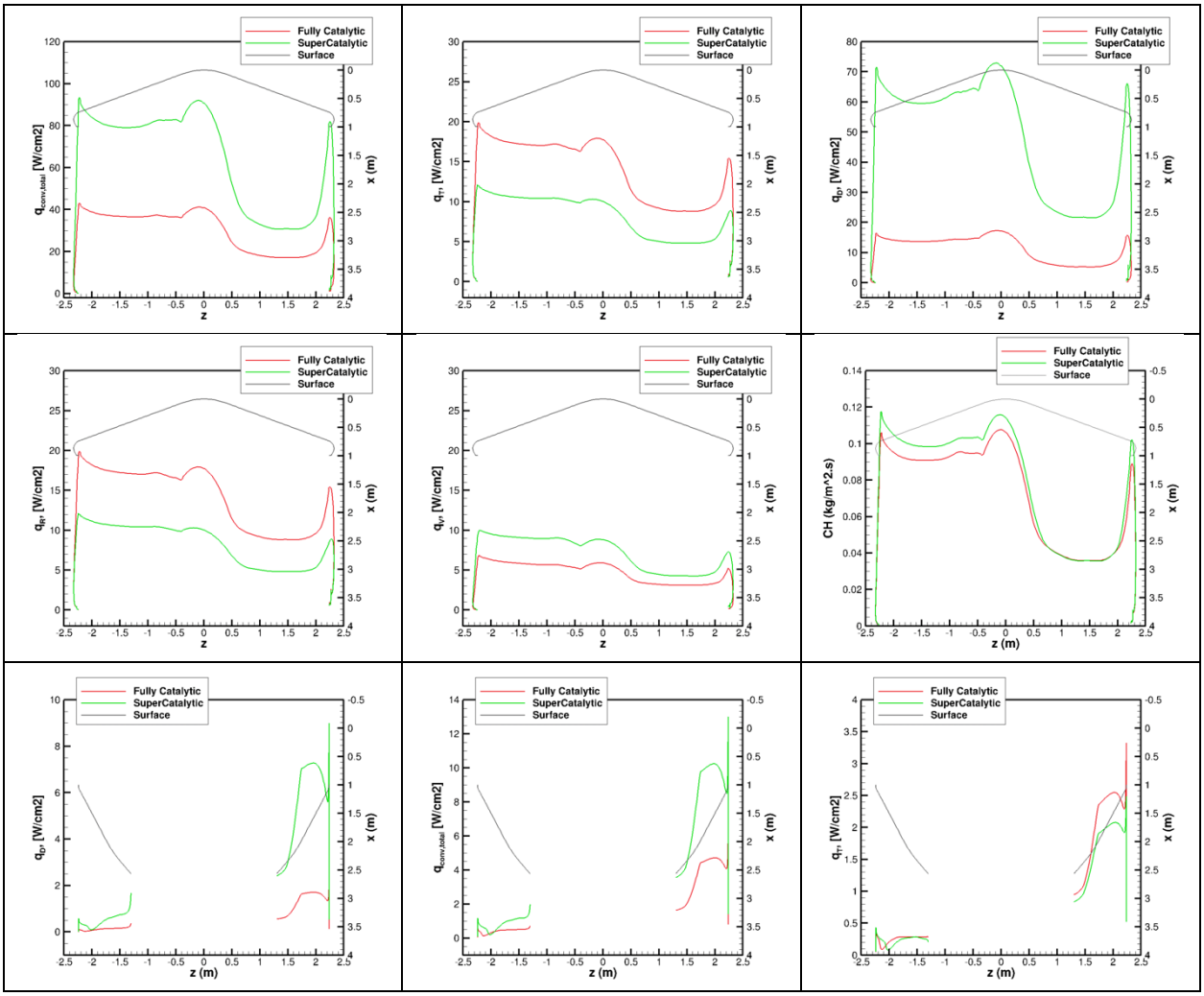

Fig. 11 Comparison of symmetry line profiles show the sensitivity to surface catalytic treatment. Total convective heat flux is the sum of convective heating due to translational, rotational, vibrational and diffusive/chemical heat fluxes. Figures in the bottom row show only the SLA-561V-covered backshell, and not the non-catalytic parachute cone and lid.
Freestream: -20 deg AoA, velocity 4.52 km/s; density 1.07057e-3 kg/m3

E. Roughness Augmentation

The heatshield TPS is aerothermally/hydraulically smooth prior to Entry Interface. During the heat pulse, the TPS material PICA is expected to undergo pyrolysis and ablation, and develop surface roughness. Historically for Mars entry[3,20], environments for heatshield TPS analysis have accounted for a roughness augmentation due to distributed roughness (small-scale features developed on the heatshield due to ablation) using empirical models and a conservative value for a representative sand-grain roughness. Current analysis for SRL borrows the framework used for MSL and Mars 2020 design, while carrying out efforts to refine both the roughness augmentation methodology, as well as the representative roughness magnitude. Roughness augmentation is computed as given below in equations (1) thru (4) – using CFD-derived smooth-wall heat flux and a pre-determined equivalent sand-grain roughness parameter (based on observations and analysis of post-test articles covered with PICA and subject to relevant heat fluxes). In these equations, smooth wall shear stress and density yield friction velocity and the friction roughness parameter k^+. Shear stress augmentation is a log linear fit on k^+, while convective heat flux augmentation is derived from a linear fit on shear stress augmentation factor. Roughness augmentation factor is assumed to be 1.0 where k^+ is below the minimum value of 10; Figure 12 shows the variation of these parameters (k^+, shear stress augmentation and heating augmentation) along the symmetry line, along with the profiles of smooth and rough wall convective heating, for an assumed equivalent sand-grain roughness of 0.6 mm.

$$U_\tau = \sqrt{\frac{\tau_w}{\rho_w}} \tag{1}$$

$$k^+ = \{\rho_w U_\tau k_s\}/\{\mu_w\} \tag{2}$$

$$\frac{\tau_{\{w,k\}}}{\tau_{w,0}} = 1 + 0.9\,(\log k^+ - 1)\ ;\ 10 < k\text{^}+ < 70 \tag{3}$$

$$\frac{q_{\{conv,k\}}}{q_{\{conv,0\}}} = 1 + 0.6\,(\frac{\tau_{\{w,k\}}}{\tau_{w,0}} - 1) \tag{4}$$

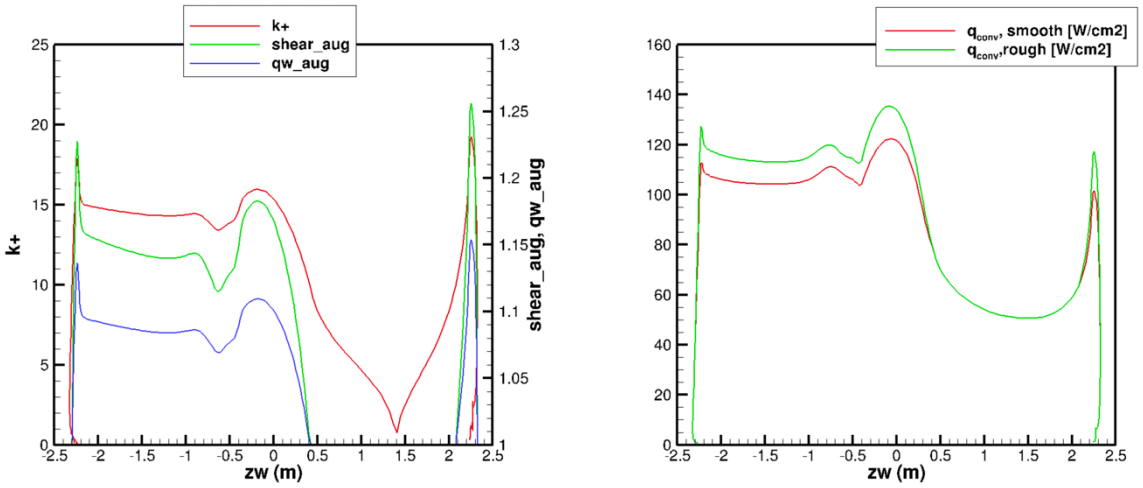

Fig. 12 Symmetry line profiles showing the parameters that go into post-CFD roughness augmentation, and the profiles of smooth and rough wall convective heating.
Freestream: AoA -20°, velocity 6.48km/s, density 7.9147e-4 kg/m3.

The heatshield TPS system is composed of multiple tiles with gap-filler in between the tiles. It is likely that during the heat pulse, the tile-tile-interfaces develop either a cavity/gap, or a fence/protrusion depending on the local environment (including pressure, heat flux, temperature and shear stress). These features (also referred to as discrete roughness features) are likely to result in a transition to turbulent flow, as well as to alter the flowfield enough to cause

local augmentation to the heating (see reference[25] for details of the analysis and the predicted augmentation factors on the aerothermal environment of MSL due to such gap fillers). Analysis for SRL does not currently account for this impact, but such accounting is planned for the future. At conditions respresentative of a Mars entry, the aft body TPS is not expected to undergo sufficient ablation to generate surface roughness, or roughness-induced augmentation to convective heating. Aft body environments are smooth-wall environments.

F. Radiation Modeling

SRL aerothermal analysis, following that of Mars 2020, includes radiative heating in the environment prediction process, on both the forebody and aft body. Radiation was neglected for MSL[3] because it was considered insignificant. Analysis and testing[26, 27] since MSL, and measurements from the Schiaparelli mission[28], drove inclusion of radiative heating analysis as part of the Mars 2020 aerothermal environment process. MEDLI2[29] aft body instrumentation (including total heat flux gauges, radiometer) validated the Mars 2020 approach and modeling of radiative heating, and confirmed that radiative heating dominates convective heating over portions of the aft body[3]. The radiative heating methodology for SRL remains largely the same as for Mars 2020. Forebody radiation calculations are performed using tangent-slab approximation, while those on the aft body use a full-angular integration procedure[30]. Radiation calculations are performed at a small subset of body points (compared to the surface CFD mesh), and are interpolated onto the surface to generate a radiation map.

Figure 13 shows contours of predicted radiative heating at six trajectory points along the 7.8 km/s trajectory, at velocities ranging from 7.3 km/s to 2.7 km/s. Note that forebody radiation has a double-peak behavior, one on either side of 6 km/s velocity. Figures show that the distribution of radiation changes through the trajectory, even as the angle of attack is constant. At higher velocities, the peak forebody radiation is on the windward side, and over the stagnation region, where as at the lower velocities, it is observed near the lee ward side. In contrast to the heatshield, aft body radiative heating shows a single pulse/peak, and magnitudes are significantly lower.

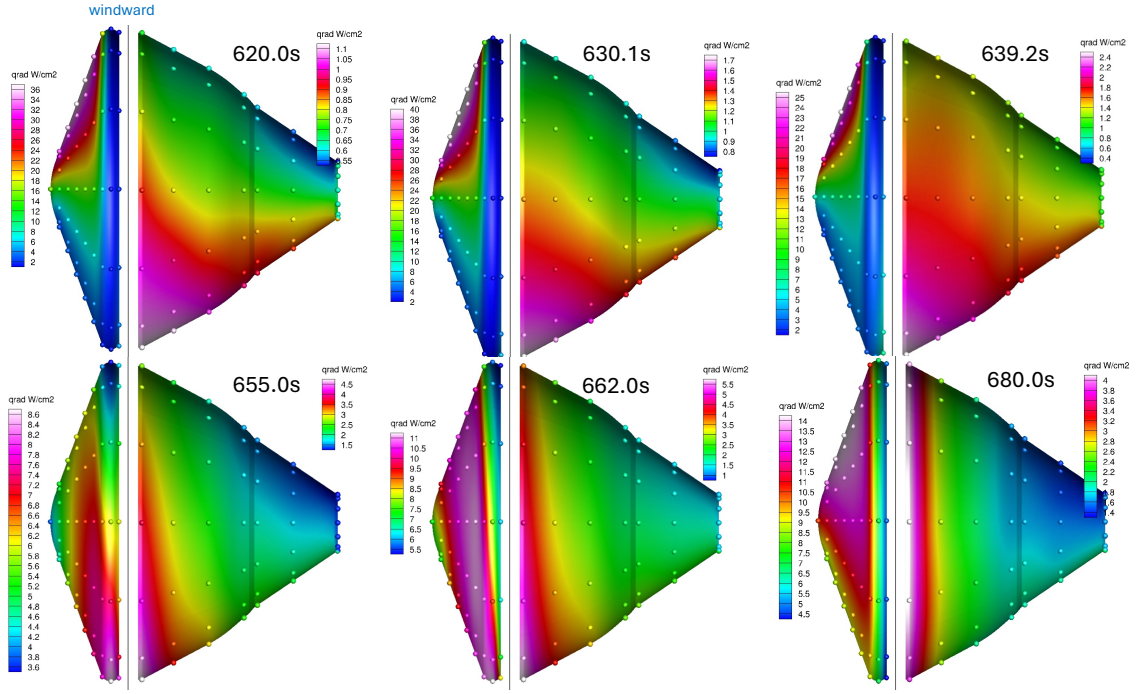

Fig. 13 Contours of radiation at different freestream conditions along the 7.8 km/s trajectory. Note that the color scales are different at each conditions, as well as for the forebody and aft body. Images on the top row correspond to freestream velocities greater than 6 km/s, those on the bottom to velocities less than 6km/s.

Both the double-peaked nature of forebody heating, and the relatively higher magnitude of radiative heating, are a consequence of the higher entry velocity. This entry velocity exposes the vehicle into newer radiative mechanisms when compared to prior missions to Mars and requires attention. Currently, a detailed investigation is underway to

justify the radiation predictions and the associated models (including the chemistry models and mechanisms in DPLR that yield the line-of-sight data, and the rate kinetics in NEQAIR) via comparison to experiments at the Electric Arc Shock Tube (EAST). The results are expected to inform future analysies, and will be presented/published in the future.

Figure 14 shows the transitions that result in radiative heating across the forebody, as a function of wavelength. The two plots correspond to freestream velocity 6.48km/s and 5.1 km/s. The former is representative of radiative physics above velocities of 6 km/s, and includes significant radiation due to CO-4th positive and CN bands. The latter, indicative of speeds below 6 km/s, indicates that radiation is largely due to CO_2 bands. Part of the investigation mentioned above will compare the spectral intensities of EAST experiments (along the lines of Ref [31]), to the predicted transitions.

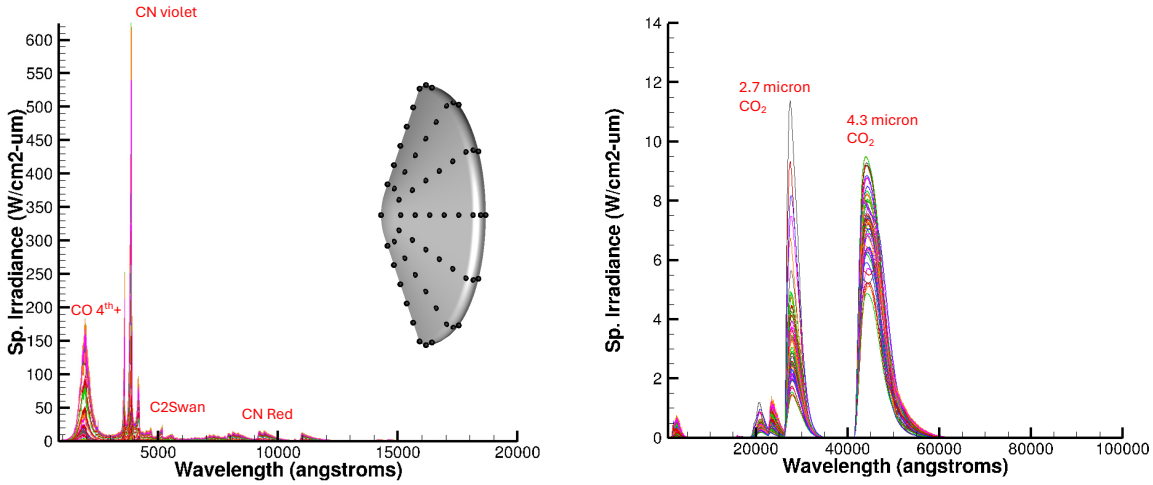

Fig. 14 Transitions resulting in forebody radiation - at conditions above (t639.2s, left) and below (t655.1s, right) 6 km/s freestream velocity.

G. Aerothermal Uncertainties

Aerothermal uncertainties (to convective and radiative heat fluxes, pressure, shear stress, film coefficient) affect both the TPS sizing analysis, as well as the TPS verification test program. SRL is currently using Mars 2020 uncertainties, even as there are changes to the underlying solvers, thermochemical models, and turbulence model. Establishment of an SRL uncertainty/margin policy is in work, and the approach incorporates ongoing comparisons against ground tests (wind tunnel data for convective heating and pressure, EAST data for radiative heating), parametric uncertainty analyses (to evaluate and include the sensitivity to modeling parameters), and code-to-code comparisons (e.g. LAURA vs DPLR, and HARA NEQAIR).

Broadly, design parameters are computed as

$$\phi_{\{design\}} = \phi_{\{prediction\}} \times \Delta\phi$$

Where $\Delta\phi$ is the uncertainty factor, usually greater than 1.0, depends on the parameter/quantity ϕ, and on the spatial location on the capsule. Table shows the uncertainty factors currently being used for SRL.

Table 3 Aerothermal Uncertainty factors currently being used for SRL

Quantity	Forebody	Aftbody
Convective heating	1.22	2.0
Film coefficient	1.22	2.0
Radiative heating	1.5	1.47
Shear stress	1.25	1.5
Pressure	1.05	1.25

IV. Predicted SRL Aerothermal Environments

This section will present results from the aerothermal analyses on the SRL geometry, and using the modeling options and parameters outlined in the previous section. Figure 15 shows surface parameters along the heatshield symmetry plane, from all the simulations along the 7.8 km/s trajectory. A few things bear mention. Simulations predict a peak unmargined stagnation pressure of nearly 55kPa, corresponding to the time of peak freestream dynamic pressure (662 seconds, or 122 seconds after Entry Interface). Peak shear stress is observed near the shoulder (region of high curvature), with (unmargined) magnitues of nearly 300 Pascals. In general, shear stress does not directly affect TPS sizing, but informs testing. Convective heating peaks at a value of 120 W/cm^2 near 639s (or 99 seconds past entry interface), and the peak convective heating is near the nose (followed closely by lee side flank). As discussed earlier, peak radiative heating is observed earlier in the heat pulse, and is highest across the windward side. Profiles indicate a peak radiative heating magnitude of 40 W/cm^2 at 630s. Finally, the design (roughwall, margined) combined heating on the heatshield is as high as 170 W/cm2 along this trajectory.

Figure 16 shows similar symmetry line profiles along the aft body. In general, windward side sees the highest pressures, shear stress and convective heating, while the leeward side sees higher radiative heating. Times of peak convective heating, radiative heating and pressure are all near the time of peak freestream dynamic pressure (662s), later than on the heatshield.

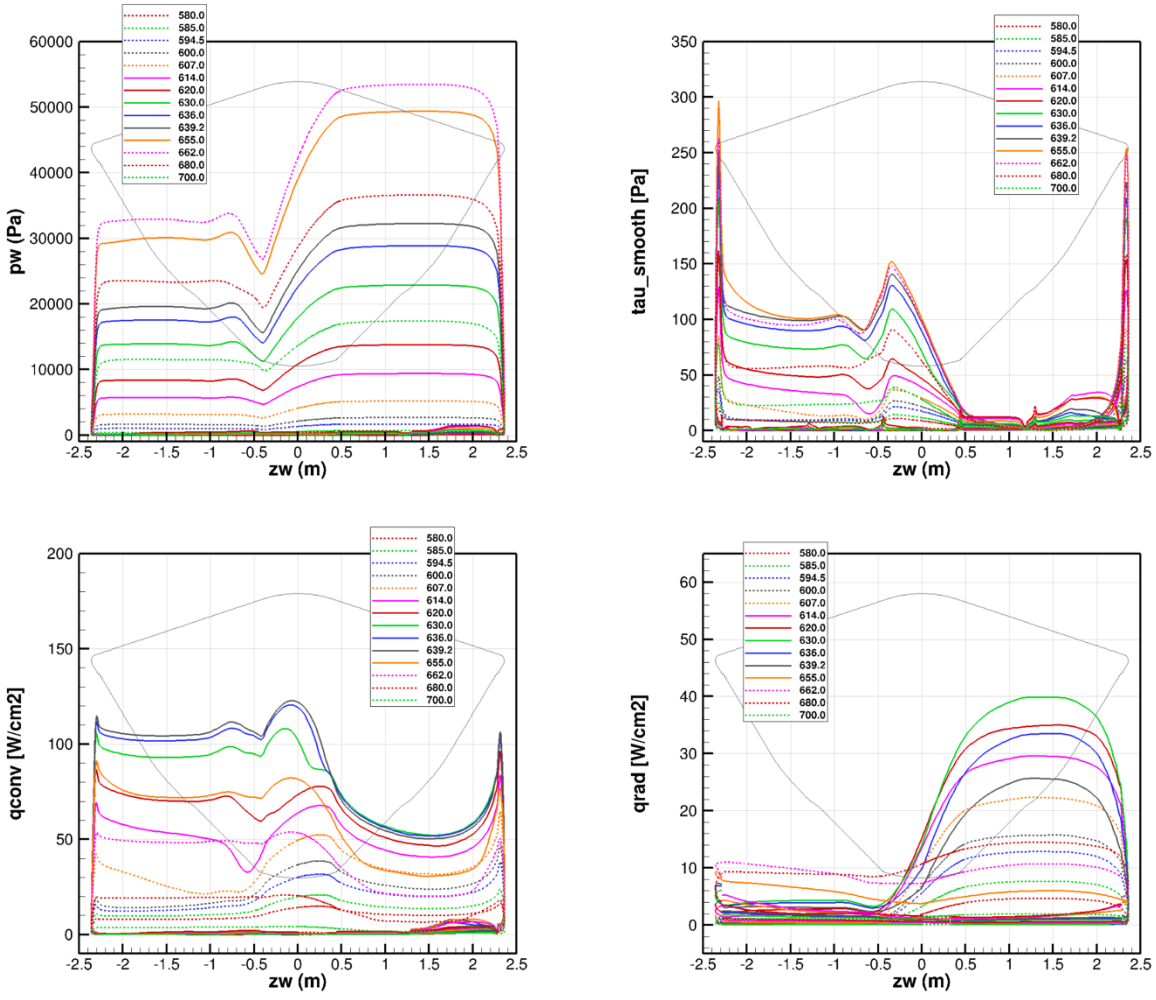

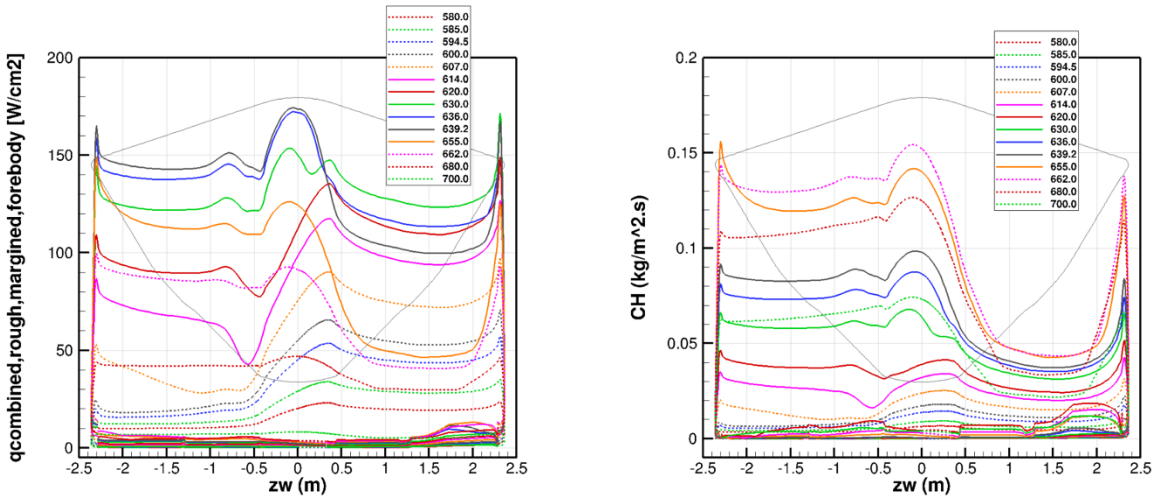

Fig. 15 Symmetry line profiles of relevant quantities, from all the CFD along the 7.8 km/s trajectory.

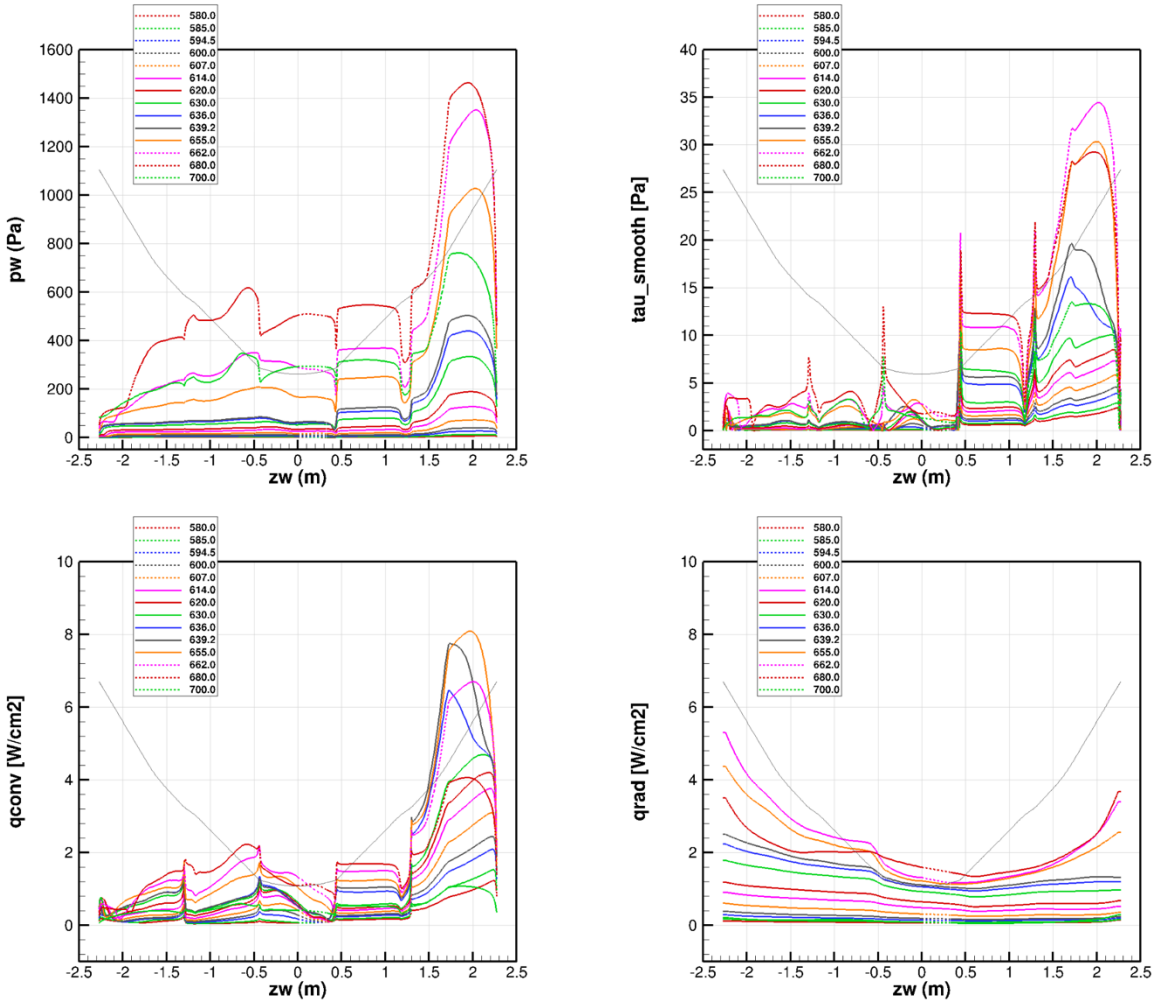

Fig. 16 Symmetryline profiles of relevant quantities on the aft body, from all the CFD along the 7.8 km/s trajectory.

As mentioned earlier, discrete CFD solutions (surface profiles) are used to generate time-traces at body points of interest, along given trajectories. This is achieved by using indicators – functions that evaluate relevant surface parameters using freestream trajectory information; the functions are established using CFD data. For example, $p_w = A\,\rho^B v^C$ where ρ and v are the freestream density and velocity along any trajectory, and A, B and C are evaluated using discrete CFD data. As can be imagined, the cofficients are particular to a given spatial location on the geometry. Figure 17 shows time traces of pressure, convective and radiative heating so evaluated, for 4 representative locations on the heatshield surface. The time-trace of radiative heating clearly shows the double-peaked nature. At the stagnation point, the magnitude of the first peak is much higher than the second one. Turbulent convective heating magnitudes at three of the four points are relatively close – consistent with the symmetry line profiles shown earlier. The parameters used towards TPS sizing include the film coefficient and edge enthalpy, and are also shown. Finally, the integrated heatload is a quantity of interest as it corelates with the TPS thickness. Note that the combined (unmargined) heat load is as high as 8000 J/cm2 (margined/design heat load is nearly 11500 J/cm2) for this trajectory, significantly higher than the that for MSL and Mars2020, or likely any other prior mission to Mars.

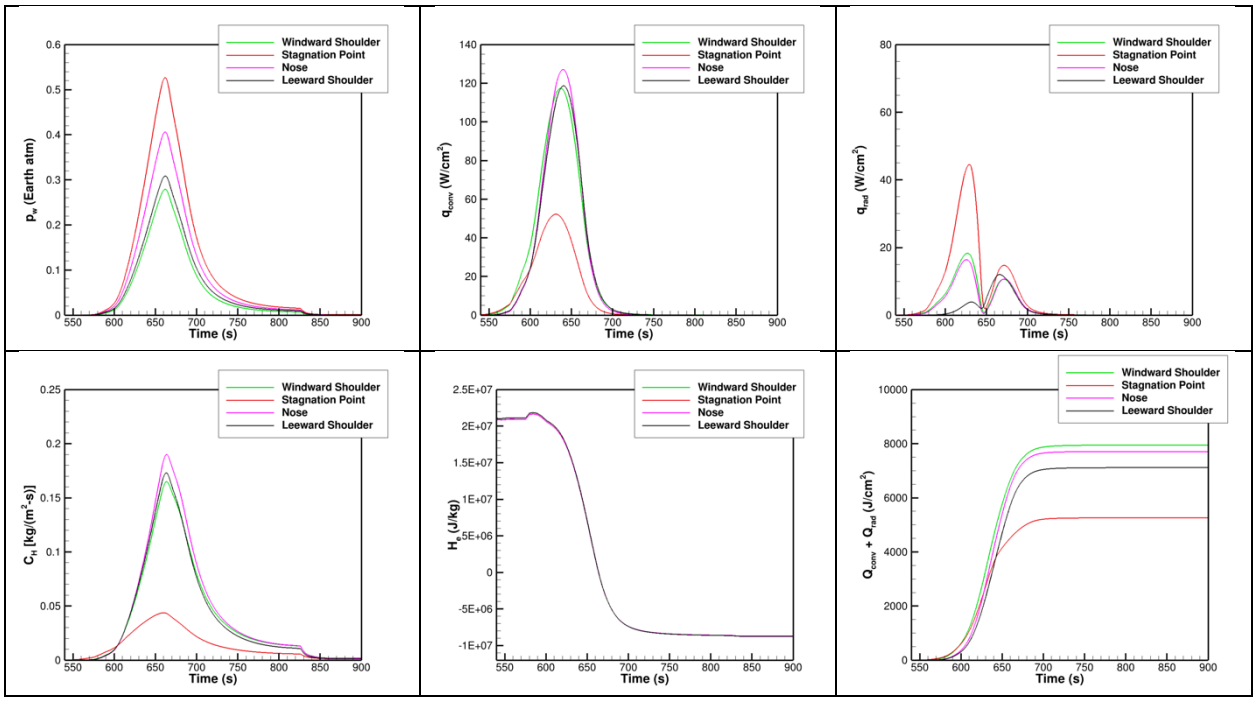

Fig. 17 Time traces of selected quantities at four different body points on the heatshield along the 7.8 km/s trajectory. Assumes fixed -20deg angle of attack.

The time traces at multiple body points are used to generate environment plots, or butterfly plots to visually represent the predicted environments across a surface, as shown in Figure 18. The plots convey the peak magnitudes of parameters of interest (margined rough-wall shear stress, combined heat flux, combined heat load) and the interplay between these parameters. Such plots are commonly used to check if the predicted environments are within the demonstrated capability of a material, and to help choose conditions for testing, with an aim to bound or cover the expected environments. Figures contrast the heatshield environments predicted along the 7.8km/s trajectory (top row) with that along the 5.4 km/s (bottom row) trajectory. The higher entry velocity results in significantly higher heat flux, and shear stress. The two trajectories have roughly the same peak pressures, as a result of their different entry flight path angles. Finally, the integrated heat load for the faster trajectory is almost three times that of the 5.4 km/s trajectory, and will influence the TPS sizing.

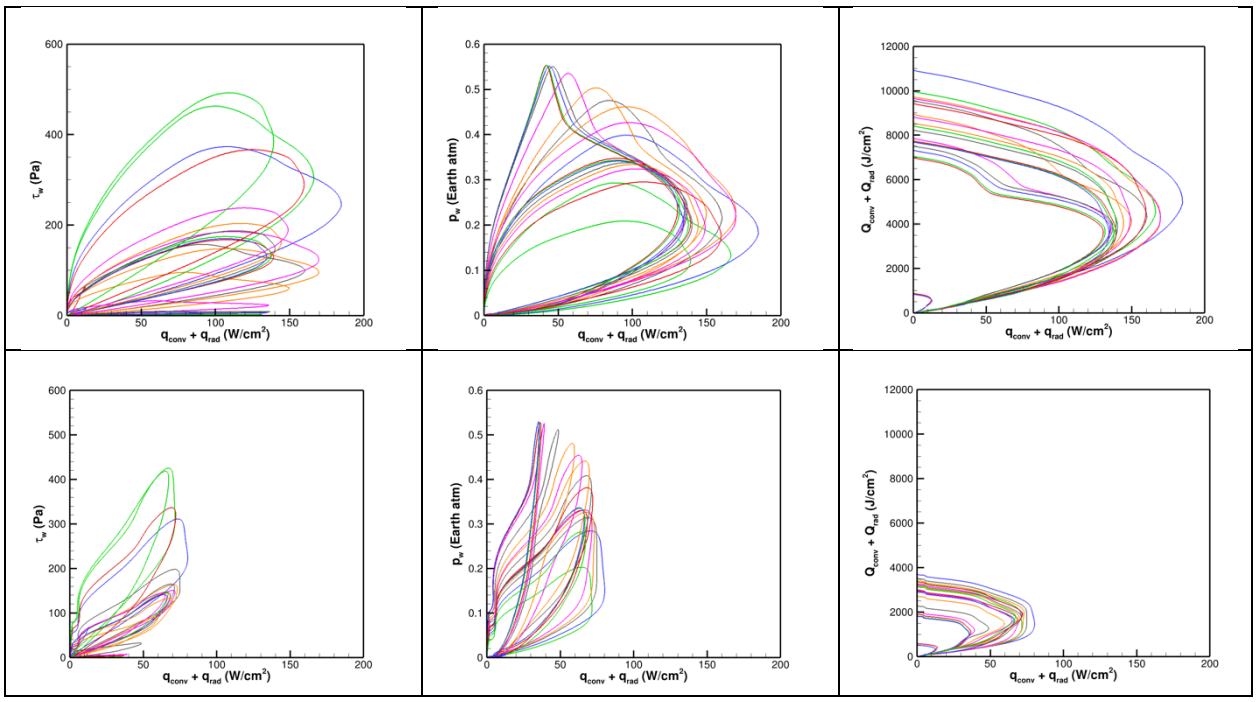

Fig. 18 Figures contrasts design environments predicted across the SRL heatshield along the 7.8 km/s trajectory (top row) and along the 5.4 km/s trajectory (bottom row) using traces at multiple body points.

Summary

Mars Sample Retrieval Lander (SRL), is one segment of the proposed Mars Sample Return Mission, the goal of which is to bring back to Earth the Martian samples being extracted by Perseverance. SRL will land the heaviest payload yet on Mars, and is being designed to be the fastest entry ever, is expected to enter the Mars atmosphere with a kinetic energy that is roughly four times that of Mars Science Laboratory (MSL) and Mars 2020.

This paper provides an overview of the aerothermal analysis process and framework used in support of the design of SRL. Largely modeled after MSL and Mars 2020, the changes to thermo-chemical modeling parameters are motivated by changes to trajectory space (entry velocity as high as 8 km/s), geometry (longer backshell that promotes more attached flow), and angle of attack (-20° compared to MSL's -16°). The faster entry velocity results in significant ionization at speeds higher than roughly 6 km/s, motivating the incorporation of an 18-species chemistry model. At these velocities (> 6 km/s) the heatshield experiences high magnitudes of radiative heating, attributed to CO and CN transitions whereas radiation below 6 km/s is attributed to CO_2 transitions. The switch to a less-conservative surface catalysis model is supported by MEDLI/MEDLI2 data, and MSL/Mars2020 post-flight reconstruction. The backshell environments assume turbulent flow, owing to the backshell geometry and angle of attack, and the resulting attached flow surface.

References

[1] B. K. Muirhead, A. Nicholas and J. Umland, "Mars Sample Return Mission Concept Status," 2020 IEEE Aerospace Conference, Big Sky, MT, USA, 2020, pp. 1-8, doi: 10.1109/AERO47225.2020.9172609.

[2] National Research Council. 2011. Vision and Voyages for Planetary Science in the Decade 2013-2022. Washington, DC: The National Academies Press. https://doi.org/10.17226/13117.

[3] Edquist, K. T., Hollis, B. R., and Johnston, C. O., "Mars Science Laboratory Heat Shield Aerothermodynamics: Design and Reconstruction," Journal of Spacecraft of Rockets, Vol. 51, No. 4, July-August 2014.

[4] A. Nelessen et al., "Mars 2020 Entry, Descent, and Landing System Overview," 2019 IEEE Aerospace Conference, Big Sky, MT, USA, 2019, pp. 1-20, doi: 10.1109/AERO.2019.8742167.

[5] Wise, A. J., Prabhu, D. K., Saunders, D. A., Johnston, C. O., and Edquist, K. T., "Computational Aerothermodynamic Environments for the Mars 2020 Entry Capsule," AIAA Paper 2018-3116, June 2018.

[6] Bose, D., White, T., Mahzari, M., and Edquist, K., “Reconstruction of Aerothermal Environment and Heat Shield Response of Mars Science Laboratory,” Journal of Spacecraft and Rockets, Vol. 51, No. 4, 2014, pp. 1174–1184.doi:10.2514/1.A32783

[7]Edquist, K. T., Mahzari, M., and Alpert, H. S., “Mars 2020 Reconstructed Aerothermal Environments and Design Margins”, AIAA Paper 2022-0553, January 2022.

[8] Mahzari, Milad & Beck, Robin & Hwang, Helen & Monk, Joshua & Morgan, Jonathan & Williams, Joseph & Edquist, Karl. (2022). Development and Sizing of the Mars2020 Thermal Protection System. 10.2514/6.2022-3951.

[9] Wright, M. J., Candler, G. V., and Bose, D., “Data-Parallel Line Relaxation Method for the Navier-Stokes Equations,” AIAA Journal, Vol. 36, No. 9, 1998, pp. 1603-1609

[10] Brandis A., Cruden B.. NEQAIR v15.0 release notes. Nonequilibrium and equilibrium radiative transport and spectra program. NASA Ames Research Center; 2020.

[11] Mazaheri, A., Gnoffo, P., Johnston, C., Kleb, B., “Laura users manual: 5.5-65135,” NASA TM 2013-217800, February 2013.

[12] Johnston, C. O., Hollis, B. R., and Sutton, K., “Spectrum Modeling for Air Shock-Layer Radiation at Lunar-Return Conditions,”Journal of Spacecraft & Rockets, Vol. 45, 2008, pp. 865–878

[13] Mitcheltree, R.A. and P.A. Gnoffo, "Wake Flow About a MESUR Mars Entry Vehicle," AIAA 94-1958, June 1994.

[14] Park, C., Howe, J.T., Jaffe, R.J., and Candler, G.V. "Review of Chemical-Kinetic Problems of Future NASA Missions, I: Mars Entries,"Journal of Thermophysics and Heat Transfer, Vol. 8, No. 1, Jan. 1994, pp. 9-23

[15] Johnston, Christopher & Brandis, A.. (2014). Modeling of nonequilibrium CO Fourth-Positive and CN Violet emission in CO2–N2 gases. Journal of Quantitative Spectroscopy and Radiative Transfer. 149. 303–317. 10.1016/j.jqsrt.2014.08.025.

[16] Baldwin, B. S., and Lomax, H., “Thin Layer Approximation and Algebraic Model for Separated Turbulent Flows,” AIAA Paper 78-0257, January 1978.

[17] Tang, C Y., Mahzari, M., Prabhu, D. K., Alpert, H. S., and Cruden, B. A. “MEDLI2: MISP Inferred Aerothermal Environment and Flow Transition Assessment”, AIAA Paper 2022-0552.

[18]Menter, F. R., “Two-Equation Eddy-Viscosity Turbulence Models for Engineering Applications,” AIAA Journal, Vol. 32, No. 8, August 1994, pp. 1598-1605.

[19] Prabhu, D. K., Rathakrishnan, B., and Muppidi, S., “An Assessment of Turbulence Models for MSR Sample Retrieval Lander Aerothermal Design”, AIAA 2024, paper in preparation

[20] Edquist, K. T., Dyakonov, A. A., Wright, M. J., and Tang, C. Y., “Aerotherodynamic Environments Definition for the Mars Science Laboratory Entry Capsule”, AIAA Paper 2007-1206.

[21]D. W. Way et al., "Mars Science Laboratory: Entry, Descent, and Landing System Performance," 2007 IEEE Aerospace Conference, Big Sky, MT, USA, 2007, pp. 1-19, doi: 10.1109/AERO.2007.352821.

[22]Wright, M. J., Tang, C. Y., Edquist, K. T., Hollis, B. R., Krasa, P., and Campbell, C. A. “A Review of Aerothermal Modeling for Mars Entry Missions”, AIAA Paper 2010-0443, January 2010.

[23] Analysis of Mars 2020 Entry Vehicle Aerothermal Flight Data Karl T. Edquist, Thomas K. West, Milad Mahzari, and Hannah S. Alpert Journal of Spacecraft and Rockets 2023 60:4, 1201-1219

[24] Ablation and Thermal Response Program for Spacecraft Heatshield Analysis Y.-K. Chen and Frank S. Milos Journal of Spacecraft and Rockets 1999 36:3, 475-483

[25] Chun Tang, Karl Edquist, Michael Wright, Steven Sepka and Alan Cassell “Numerical Simulations of Protruding Gapfillers on the Mars Science Laboratory Heatshield”, AIAA Paper 2009-4077.

[26] Brandis, A. & Johnston, Christopher & Cruden, Brett & Prabhu, Dinesh & Wray, Alan & Liu, Yen & Schwenke, David & Bose, Deepak. (2013). Validation of CO 4th Positive Radiation for Mars Entry. Journal of Quantitative Spectroscopy and Radiative Transfer. 121. 91–104. 10.1016/j.jqsrt.2013.02.009.

[27] Brandis, A.M., Saunders, D. A., Johnston, C. O., Cruden, B. A., and White, T. R., "Radiative heating on the After-Body of Martian Entry Vehicles", Journal of Thermophysics and Heat Transfer, Vol 34, #1, 2020.

[28] Gülhan, Ali & Thiele, Thomas & Siebe, Frank & Kronen, Rolf & Schleutker, Thorn. (2018). Aerothermal Measurements from the ExoMars Schiaparelli Capsule Entry. Journal of Spacecraft and Rockets. 56. 1-14. 10.2514/1.A34228.

[29] Miller, R. A., Tang, C. Y., White, T.R., and Cruden, B.A., "MEDLI2: MISP Measured Aftbody Aerothermal Environment", AIAA Paper 2022-0551.

[30] Brandis, A. J., Saunders, D. A., Johnston, C.O., Cruden, B. A., and White, T.R., "Radiative Heating on the After-Body of Martian Entry Vehicles", JTHT, vol 34, issue 1.

[31] Augustin C. Tibère-Inglesse Brett A. Cruden Christopher Jelloian and Raymond M. Spearrin, "Examination of Mars2020 shock-layer conditions via infrared emission spectroscopy of CO2", AIAA Paper 2023-0960